International Journal of Nanomedicine

Dovepress
open access to scientific and medical research

Open Access Full Text Article

ORIGINAL RESEARCH

Nano-Photosensitizer Directed Targeted Phototherapy Effective Against Oral Cancer in Animal Model

Lina Yu[1,*], Guanxiong Zhu[1,*], Zeyu Zhang[1,*], Zidan Xu[1], Weijie Peng[1,2], Liting Zeng[1], Yang Yu[3], Siran Wang[1], Zhongxiao Lin[1,2,4], Xin Zhang[4], Na Zhou[4], Lingmin Zhang[1,2], Lu Liang[1,2]

[1]Department of Preventive Dentistry, Affiliated Stomatology Hospital of Guangzhou Medical University, Guangdong Engineering Research Center of Oral Restoration and Reconstruction, Guangzhou Key Laboratory of Basic and Applied Research of Oral Regenerative Medicine, Guangzhou, 510182, People's Republic of China; [2]Guangzhou Municipal and Guangdong Provincial Key Laboratory of Molecular Target & Clinical Pharmacology, the State & NMPA Key Laboratory of Respiratory Disease, School of Pharmaceutical Sciences & the Fifth Affiliated Hospital, Guangzhou Medical University, Guangzhou, 511436, People's Republic of China; [3]Department of Sports and Health, Guangzhou Sport University, Guangzhou, People's Republic of China; [4]State Key Laboratory of Quality Research in Chinese Medicine, Macau University of Science and Technology, Avenida Wailong, Taipa, Macau, People's Republic of China

*These authors contributed equally to this work

Correspondence: Lingmin Zhang; Lu Liang, Email zhanglm@gzhmu.edu.cn; lliangaa@gzhmu.edu.cn

Background: Photodynamic therapy (PDT) has emerged as a promising strategy for oral cancer treatment. Verteporfin is a powerful photosensitizer and widely used in the treatment of macular degeneration. However, rare work has reported its potential in the treatment of oral cancer.

Methods: In this study, we introduce an innovative approach of nano-photosensitizer based on Verteporfin, which was prepared by utilizing macrophage membrane to coat Verteporfin-loaded zeolitic imidazolate framework 8 (ZIF-8) for effective photodynamic therapy against oral cancer. Nanoparticle characteristics were assessed including size, zeta potential, and PDI. Cellular uptake studies were conducted using CAL-27 cells. Furthermore, inhibitory effects in both in vitro and in vivo settings were observed, ensuring biosafety. Assessment of anticancer efficacy involved tumor volume measurement, histological analyses, and immunohistochemical staining.

Results: In vitro experiments indicated that the nano-photosensitizer showed efficient cellular uptake in the oral cancer cells. Upon the laser irradiation, the nano-photosensitizer induced the generation of reactive oxygen species (ROS), leading to cancer cell apoptosis. The in vivo experiments indicated that the coating with cell membranes enhanced the circulation time of nano-photosensitizer. Moreover, the specificity of the nano-photosensitizer to the cancer cells was also improved by the cell membrane-camouflaged structure in the tumor-bearing mouse model, which inhibited the tumor growth significantly by the photodynamic effect in the presence of laser irradiation.

Conclusion: Overall, our findings demonstrate the potential of macrophage membrane-coated ZIF-8-based nanoparticles loaded with Verteporfin for effective photodynamic therapy in oral cancer treatment. This nano-system holds promise for synergistic cancer therapy by combining the cytotoxic effects of PDT with the activation of the immune system, providing a novel therapeutic strategy for combating cancer.

Keywords: photodynamic therapy, verteporfin, oral cancer, macrophages, zeolitic imidazolate framework 8

Introduction

Tongue squamous cell carcinoma (TSCC) is a prevalent and highly fatal form of oral cancer.[1] This cancer type is marked by a grim prognosis, frequent lymphatic metastasis (spread to nearby lymph nodes), and a notable rate of regional recurrence. The conventional treatment protocol for TSCC entails surgery, followed by postoperative radiotherapy and chemotherapy. Nonetheless, despite these treatments, the 5-year overall survival rate for TSCC has not exhibited

Received: 8 September 2023
Accepted: 22 October 2023
Published: 1 November 2023

significant enhancement in recent years.[2] Therefore, it is imperative to formulate precise and personalized treatment strategies.

Verteporfin, marketed as Visudyne and approved by the FDA, is primarily employed for the treatment of specific severe eye conditions, notably age-related macular degeneration (AMD). Beyond its ophthalmic use, preclinical investigations have unveiled the potential utility of verteporfin in cancer therapy, encompassing liver, pancreatic, gastric, and head and neck cancers.[3–7] In the realm of cancer research, Verteporfin is under scrutiny as a photosensitizer for photodynamic therapy, holding promise as a modality for cancer treatment. In this approach, the drug is administered systemically, and when activated by specific wavelengths of light, it generates reactive oxygen species that can cause localized cell damage and destruction of tumor tissue. Clinical trials and preclinical studies are underway to investigate the efficacy, safety, and optimal use of Verteporfin and related compounds in treating cancers. However, rare work was reported on the treating oral cancer with Verteporfin-based formulations.

Biomimetic nanoparticles, formed by enveloping nanoparticles with natural cell membranes, represent a promising approach to enhance targeted drug delivery. These nanoparticles capitalize on the distinctive attributes of cell membranes to enhance their functionality and interactions within biological systems.[8,9] Macrophages, as immune cells, play a pivotal role in engulfing foreign particles. Recent research suggests that macrophages contribute to immune regulation in tumor cells, augmenting tumor phagocytosis and reinforcing their capacity to inhibit tumor growth and metastasis.[10] By coating nanoparticles with macrophage membranes, the nanoparticles can mimic the characteristics of macrophages, which can provide several advantages: prolonged in vivo circulation, reduced immunological surveillance, and enhanced tumor homing.[11–14] Once the camouflaged nanoparticles reach the tumor sites, they selectively bound to various tumor cells, which was beneficial for cancer therapy.[11,15]

Metal-organic frameworks (MOFs) represent a class of hybrid materials formed by combining metal cations with organic bridging ligands.[16] These structures possess a porous framework with customizable composition and pore sizes, rendering them versatile for various applications, including drug delivery systems and nanotheranostics.[17] Additionally, MOFs have been engineered as nanocatalysts to trigger the production of oxidizing radicals, such as hydroxyl (•OH) radicals, specifically within cancer cells.[18] This approach selectively induces cytotoxicity in cancer cells while sparing healthy tissues. Furthermore, MOFs have been harnessed as sonosensitizers, capable of generating reactive oxygen species (ROS) or oxygen within tumor environments, thereby enhancing the efficacy of specific cancer therapies.[15,19] One noteworthy MOF in this context is zeolitic imidazolate framework 8 (ZIF-8), prized for its thermal stability and lower toxicity compared to other MOFs, making it well-suited for drug delivery applications.[20] Notably, ZIF-8 exhibits biodegradability and controlled cargo release properties due to its limited stability in aqueous conditions.[21] However, these characteristics of ZIF-8 can present challenges for targeted delivery, as they may lead to cargo leakage when exposed to aqueous conditions before reaching the intended site of action.[22]

In this study, we developed a biomimetic vehicle for cancer therapy by camouflaging M1 macrophage-derived membranes onto a metal-organic framework (MOF)-based platform, which was used to carry Verteporfin. This type of nano-photosensitizer was expected to show enhanced circulation lifetime, specificity to the oral cancer cells, and inducing effective photodynamic effect to treat oral cancer cells. This strategy provides a promising platform for oral cancer therapy.

Materials and Methods

2-methylimidazole (99%) and zinc nitrate hexahydrate ($Zn(NO_3)_2 \cdot 6H_2O$, 98%) were from Sigma-Aldrich (USA), and Verteporfin was purchased from MedChemExpress (China). Fetal bovine serum (FBS) was purchased from ExCell Bio (China). Phosphate buffer saline (PBS), penicillin, and streptomycin were purchased from Gibco (USA).

Cell Culture Studies Using Different Cell Lines

The human tongue squamous cell carcinoma cell line CAL-27 was obtained from Wuhan Procell Life Technology Co. LTD (Wuhan, China) and incubated in Dulbecco's Modified Eagle Medium: F-12 (DMEM/F-12) (Gibco, USA) supplemented with 10% FBS and 1% Penicillin/Streptomycin in 5% CO2 at 37 °C. The mouse macrophage cell line

(Raw 264.7 cells) was purchased from the Shanghai Institute of Cell Biology (Shanghai, China) and cultured in DMEM medium (Gibco, USA) supplemented with 10% FBS and 1% Penicillin/Streptomycin in 5% CO_2 at 37 °C.

Synthesis of ZIF-8@Verteporfin

Verteporfin (2 mg/mL) was prepared by dissolving it in a mixture containing 2-methylimidazole (200 mg/mL) in methanol. This solution was then stirred for a duration of 10 min. Subsequently, Zn (NO3)2·6H2O (100 mg/mL) was introduced while maintaining stirring. This mixed system was stirred in darkness at room temperature for 1 h. ZIF-8@Ver was then isolated from the dispersion through centrifugation (12,000 rpm, 5 min), and finally stored at 4°C.

Preparation of ZIF-8@ Verteporfin - M1 Macrophages

ZIF-8@Ver was coated with cell membranes extracted from M1 macrophages (M1M), following a previously established protocol.[23] To summarize, M1M and ZIF-8@Ver were combined at a weight ratio of 5/1, subjected to a 5-minute ultrasound treatment, and subsequently extruded to yield ZIF-8@Ver-M1M.

Characterization of the Nanoparticles

The polydispersity index (PDI), particle size, and zeta potential of ZIF-8 nanoparticles, ZIF-8@Ver, and ZIF-8@Ver-M1M were assessed by Nano ZS instrument (Malvern, UK). Prior to measurement, the samples were pre-diluted with deionized water at a 3:7 ratio (v/v) to achieve low ion intensity and consistent surface charges. Transmission electron microscopy (TEM) The images were observed by transmission electron microscopy (TEM) (JEOL, Japan). For characterizing M1 macrophage membrane proteins, a sodium dodecyl sulfate-polyacrylamide gel electrophoresis (SDS-PAGE) assay was performed.

Drug Loading Efficiency (DLE) and Drug Loading Content (DLC)

ZIF-8@Ver was synthesized via the "one-pot" method, followed by centrifugation at 12,000 rpm for 5 min at 4°C. In parallel, ZIF-8 was prepared using the same method but without the addition of Verteporfin, serving as a blank control. The loading efficiency of Verteporfin was determined by UV-Vis spectrophotometry (Spectrum, SP1920, China) and calculated by this formula: Verteporfin encapsulation efficiency (%) = (Amount of loaded Verteporfin) / (Amount of added Verteporfin) * 100%.

For the quantification of drug loading content, ZIF-8@Ver was freeze-dried and pH-adjusted to 5.0 until complete nanoparticle degradation. The loading content was then assessed using the following equation: Drug loading content (DLC) (%) = (Weight of loaded drugs) / (Weight of nanoparticles) * 100%.

In vitro Drug Release

ZIF-8@Ver-M1M was prepared and subsequently enclosed within a dialysis bag with a cutoff of 3500 Da. Two separate dialysis bags at two distinct pH levels (pH = 5.0 and 7.4) were prepared. These bags were then subjected to incubation for various time points (0, 1, 2, 4, 6, 8, 12, 24, 36, 48, 72, and 96 h). To determine the Verteporfin content, absorbance measurements were conducted using a Multifunctional microporous plate detector (BioTek, USA).

In vitro Cellular Uptake

CAL-27 cells were exposed to varying concentrations of ZIF-8@Ver-M1M nanoparticles (1, 2, 3, 4, 5 μg/Ml) in F12 medium for 24 hours. Afterward, they were subjected to staining with DAPI and Actin-Tracker Green. To explore the temporal dynamics of cellular nanoparticle uptake (1, 2, 4, 6, and 8 hours), the same method was used. The cellular uptake was observed by confocal laser scanning microscopy (CLSM, LSM880, Zeiss, Germany).

Flow Cytometry (FACS) analysis was carried out to quantitatively assess cellular uptake. CAL-27 cells were treated with varying concentrations of ZIF-8@Ver-M1M nanoparticles (1, 2, 3, 4, 5 μg/mL). Similarly, the temporal uptake dynamics (1, 2, 4, 6, and 8 hours) were explored using the same procedure. The cells were subsequently detached using 0.25% trypsin and resuspended in 100 μL PBS.

Lysosome Escape Assay

To assess the intracellular release of Verteporfin, a lysosome escape experiment was conducted. CAL-27 cells were then treated with ZIF-8@Ver-M1M (Verteporfin, 5 μg/mL). Following incubation for specified time intervals (1 hour and 4 hours), the cells were stained with Lyso-Tracker Blue DND-22 (Thermo Fisher, USA). The nanoparticle distribution within the cells at the different time points were examined by CLSM.

Assessment of Reactive Oxygen Species (ROS) Generation

To assess the induction of reactive oxygen species (ROS) by various formulations, we utilized a reactive oxygen species assay kit (BestBio, China). CAL-27 cells were cultured in confocal dishes and exposed to different treatments: PBS, Verteporfin with Laser (Ver+Laser), ZIF-8@Ver with Laser (ZIF-8@Ver+Laser), and ZIF-8@Ver-M1M with Laser (ZIF-8@Ver-M1M+Laser) for 4 hours. To detect ROS production, cells were treated with 10 μM of 2',7'-Dichlorodihydrofluorescein diacetate (DCFH-DA) for 30 min. Afterward, the cells were rinsed with FBS-free DMEM/F-12 to remove any DCFH-DA that had not entered the cells. For groups exposed to laser treatment, irradiation was performed using a 660 nm laser at 2 W/cm2 for 5 minutes. Fluorescence was observed using CLSM with excitation at 488 nm and emission at 525 nm.

In vitro Cytotoxicity Assays

To assess nanoparticle toxicity in vitro, the Live/Dead Cell Staining Kit was employed. CAL-27 cells were seeded at a density of 1×105 cells per well in confocal dishes and allowed to incubate for 24 hours. Following this, cells were treated with either Verteporfin, ZIF-8@Ver, or ZIF-8@Ver-M1M for 4 hours, with PBS-treated cells serving as the control. Subsequently, the cells were stained with Calcein-AM/PI (Beyotime, China) for CLSM observation.

The cytotoxicity of Verteporfin, ZIF-8@Ver, or ZIF-8@Ver-M1M in CAL-27 cells was assessed using the Cell Counting Kit-8 (CCK-8) assay. Various formulations (PBS, Verteporfin, ZIF-8, ZIF-8@Ver, or ZIF-8@Ver-M1M) were then added to the respective wells and incubated for 4 hours. Cell viability was determined through the CCK-8 assay and quantified using a multifunctional plate reader (BioTek, USA).

In vivo Anticancer Study

Thirty female BALB/c nude mice, aged 5–6 weeks and weighing approximately 18–22 g, were randomly divided into six groups with five mice in each group and maintained in a specific pathogen-free environment. All animal experiments were conducted in accordance with the guidelines of the Institutional Authority for Laboratory Animal Care at Guangzhou Medical University (S2023-511).

The tumor model was induced through the injection of CAL-27 cells. After 2 weeks, tumor-bearing mice were randomly assigned to one of six groups: PBS, Verteporfin, ZIF-8@Ver, ZIF-8@Ver-M1M, ZIF-8@Ver+laser, and ZIF-8@Ver-M1M+laser. Local injections of the respective formulations were administered every 2 days. ZIF-8@Ver+laser and ZIF-8@Ver-M1M+laser were exposed to laser treatment, irradiation was performed using a 660 nm laser at 2 W/cm^2 for 5 min. Tumor volumes were measured every 2 days. After five treatment cycles, the mice were euthanized. To evaluate the acute toxicity of the therapeutic agents, the major organs and tumors were harvested and fixed. Tumor volume was calculated according to the previously described protocols.[23–25]

In vivo Evaluation of Biodistribution

After successfully establishing the animal model, Verteporfin, ZIF-8@Ver, or ZIF-8@Ver-M1M were synthesized and locally administered to the tumor-bearing mice. Anesthesia was induced with 2% isoflurane, and the mice were imaged at predetermined intervals (1, 2, 4, 8, 12, 24, and 48 hours) using the In Vivo Imaging System (PerkinElmer, IVIS Lumina LT, USA). Fluorescence data were subsequently analyzed with Living Image Software.

Hematoxylin-Eosin (HE) Staining

The major organs and tumors were subjected to a multigradient dehydration process using ethanol, followed by paraffin embedding, sectioning, and hematoxylin and eosin (HE) staining. Analysis of histological characteristics was performed using Aperio Digital Pathology (Leica, Italy) for biopsy observation and assessment.

dT-Mediated dUTP Nick-End Labeling (TUNEL) Assay

Tumors were fixed in 4% paraformaldehyde and subsequently paraffin-embedded. Tissue sections of 5 μm thickness were then employed for TUNEL analysis. Apoptotic cells in various experimental groups were identified using a cell death detection kit (Roche, USA).

Immunohistochemical Staining

The tumors underwent fixation in 4% paraformaldehyde and subsequent paraffin embedding. Additional IHC staining with anti-Ki67 antibody staining was used to analyze protein expression. Aperio Digital Pathology (Leica, Italy) was used to observe and analyze the histological characteristics.

Statistical Analysis

Data were expressed as means ± S.E. Statistical comparisons among groups were conducted using one-way analysis of variance (ANOVA), and Tukey's multiple comparisons test (GraphPad) was employed subsequently. Statistical significance was defined as $p < 0.05$.

Results

The Construction and Characterization of Nanoparticles

The materials were synthesized and examined using transmission electron microscopy (TEM). TEM images confirm the rhombic dodecahedral three-dimensional structure of the synthesized ZIF-8 and ZIF-8@Ver, displaying sharp edges (Figure 1A and B). However, the morphology of ZIF-8@Ver-M1M appeared less regular and the angles became blurred, indicating successful loading and surface modification by macrophage membrane (Figure 1C). TEM images of ZIF-8, ZIF-8@Ver, ZIF-8@Ver-M1M reveal uniformly dispersed nanoparticles with average diameters of 186.4 ± 5.8 nm, 192.6 ± 2.3 nm, 210 ± 8.3 nm, respectively (Figure 1D-F). The zeta potential of ZIF-8@Ver was 35.6 mV, which was increased from 26.2 mV corresponding to ZIF-8. After coating with M1 macrophage-derived membranes, the zeta potential of prepared nanoparticles decreased to −20.3 ± 5.6 mV (Figure 1G). The loading efficiency at different verteporfin contents in ZIF-8@Ver was calculated by UV-vis spectroscopy analysis (Figure 1H). The ratio of ZIF-8 to verteporfin at 100 was optimized for the further study, and the loading efficiency was nearly 60%. Sodium dodecyl sulphate-polyacrylamide gel electrophoresis (SDS-PAGE) analysis demonstrated that ZIF-8@Ver-M1M preserved a significant portion of the protein constituents from macrophage membrane (Figure 1I). The preservation of proteins may contribute to the biocompatibility of ZIF-8@Ver and selectively delivery. The findings indicated successful coating of macrophage membranes onto the MOF-based complexes, resulting in the formation of bioinspired nanoparticles.

Evaluation of Cellular Uptake

The cellular uptake of ZIF-8@Ver-M1M was evaluated at different time points and dosages to understand its uptake kinetics and dose-dependent behavior in CAL-27 cells. For the cellular uptake analysis, CAL-27 cells were treated with varying concentrations of ZIF-8@Ver-M1M nanoparticles (1, 2, 3, 4, and 5 μg/mL) and incubated for different time durations (1, 2, 4, 6, and 8 h). The cellular uptake of ZIF-8@Ver-M1M was assessed by confocal laser scanning microscope (CLSM) and FACS analysis. The CLSM images revealed that the cellular uptake of ZIF-8@Ver-M1M increased with both time and dosage. At the initial time points (1 and 2 h), a minimal fluorescence signal was observed, indicating a low uptake of nanoparticles by the cells. However, as the incubation time increased to 4, 6, and 8 h, a significant increase in fluorescence intensity was observed, suggesting enhanced cellular uptake of ZIF-8@Ver-M1M (Figure 2A). Furthermore, the dosage-dependent cellular uptake analysis indicated that the fluorescence intensity within

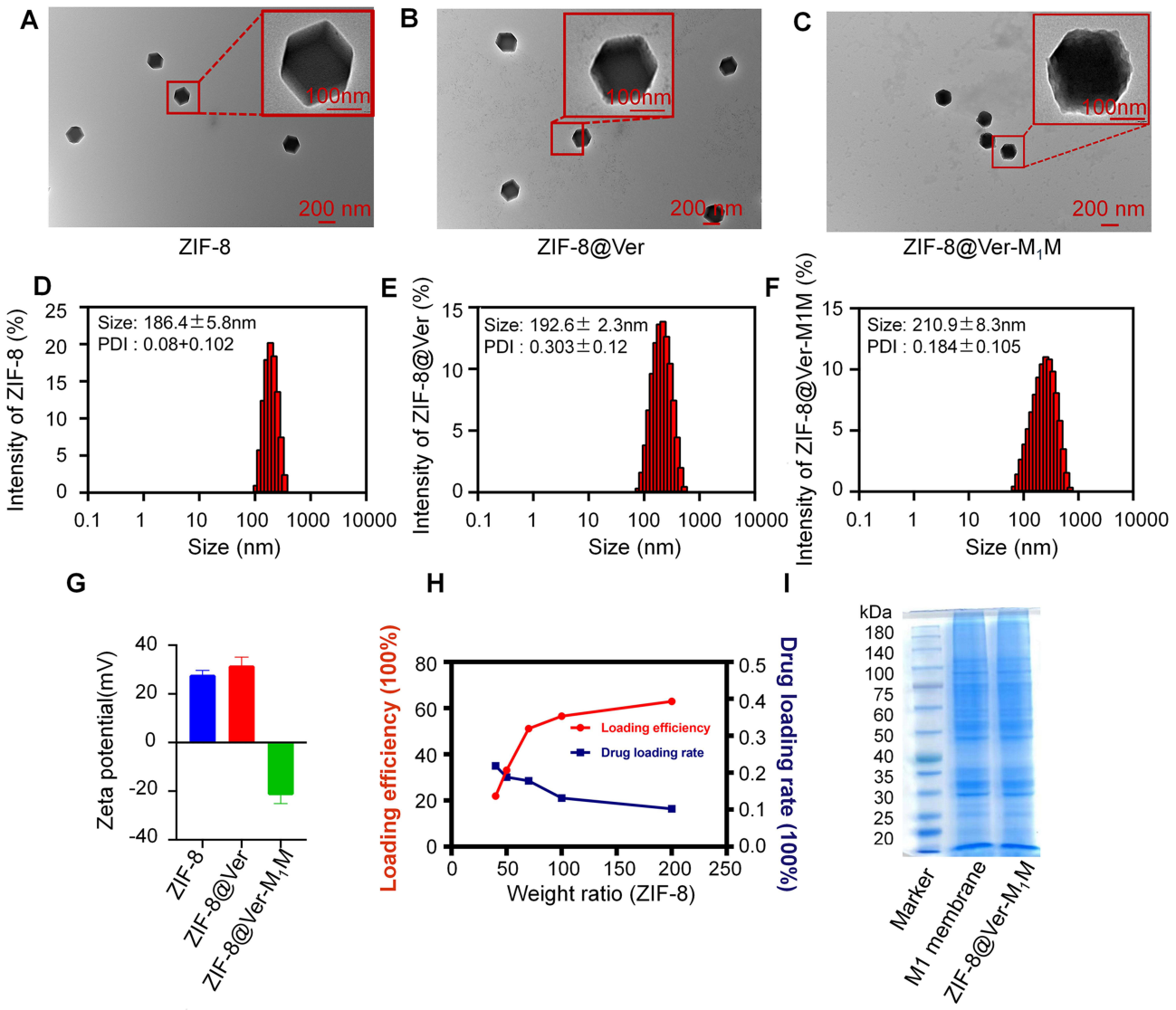

Figure 1 Characterizations of M1 macrophage membrane-coated MOF-based nanoparticles. (**A-C**) TEM image analysis of ZIF-8, ZIF-8@Ver and ZIF-8@Ver-M1M. (**D-F**) The size distribution of ZIF-8, ZIF-8@Ver and ZIF-8@Ver-M1M. (**H**) Loading efficiency by ZIF-8/verteporfin nanoparticles. (**I**) Protein composition analysis by SDS-PAGE.

the cells increased with the concentration of ZIF-8@Ver-M1M (Figure 2B). This indicates that the uptake of ZIF-8@Ver-M1M nanoparticles by CAL-27 cells is dosage-dependent. Overall, the results indicate that the cellular uptake of ZIF-8@Ver-M1M in CAL-27 cells is both time- and dosage-dependent. These findings suggest that longer incubation times and higher nanoparticle concentrations can lead to increased uptake of ZIF-8@Ver-M1M by cancer cells, potentially enhancing its therapeutic efficacy in photodynamic therapy. Thus, ZIF-8@Ver-M1M at a concentration of 5 μg/mL Ver and transfection for 8 h were used in subsequent experiments.

The lysosome escape ability of ZIF-8@Ver-M1M nanoparticles was investigated to assess their capability to evade lysosomal degradation and release the encapsulated Verteporfin within the CAL-27 cells. CLSM was used to detect the distribution of ZIF-8@Ver-M1M within the cells and evaluate their escape from the lysosomal compartment. The CLSM images demonstrated that in the early time point (1 hour), the blue fluorescence from the Lyso-Tracker dye and the red fluorescence from ZIF-8@Ver-M1M nanoparticles largely overlapped, indicating that the nanoparticles were localized within the lysosomes (Figure 2C). However, as the incubation time increased to 4 h, a distinct decrease in the co-localization of blue and red fluorescence was observed. This suggests that a significant fraction of ZIF-8@Ver-M1M successfully escaped from the lysosomes, leading to reduced overlap between the lysosomal compartment and

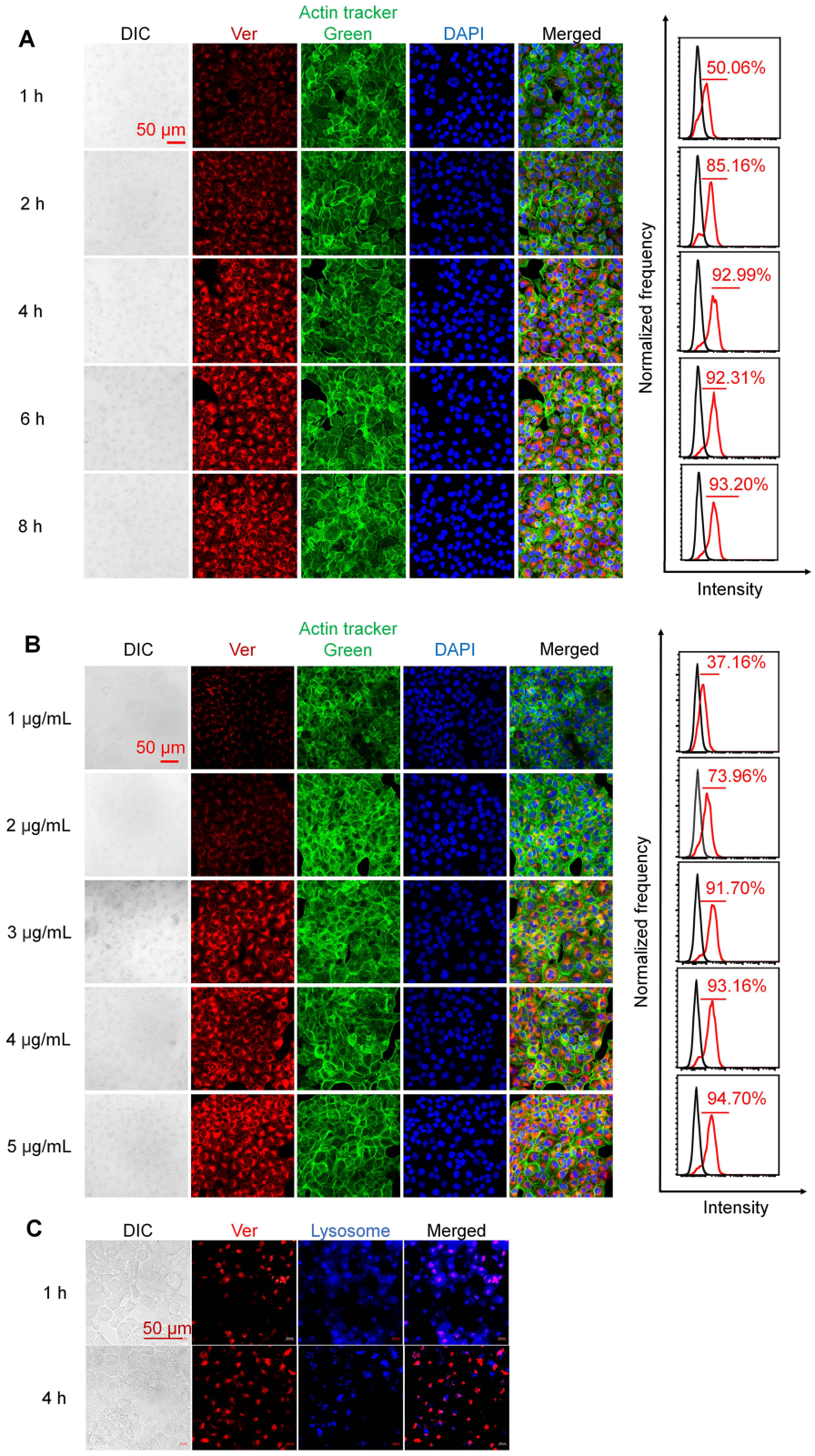

Figure 2 Cellular uptake of ZIF-8@Ver-M1M under different conditions. (**A**) CAL-27 cells were transfected for different time points. (**B**) CAL-27 cells were transfected with different concentrations of ZIF-8@Ver-M1M. (**C**) Lysosome escape of ZIF-8@Ver-M1M.

Verteporfin. The results indicate that ZIF-8@Ver-M1M nanoparticles can escape from the lysosomal compartment over time. This lysosome escape is crucial for effective drug release and subsequent intracellular action of Verteporfin, enhancing its photodynamic therapy efficacy against CAL-27 cancer cells. Overall, these findings highlight the potential of ZIF-8@Ver-M1M nanoparticles to overcome lysosomal entrapment and facilitate efficient drug release, further supporting their application in photodynamic therapy for cancer treatment.

In vitro Assessment of Antitumor Potential

The cytotoxicity of both ZIF-8@Ver and ZIF-8@Ver-M1M was evaluated in CAL-27 cells. Following treatment with either ZIF-8@Ver in combination with laser (ZIF-8@Ver + Laser) or ZIF-8@Ver-M1M in conjunction with laser (ZIF-8@Ver-M1M + Laser), the viability of CAL-27 cells markedly diminished compared to the groups that did not receive laser treatment. Notably, a more pronounced synergistic effect was observed when combining ZIF-8@Ver-M1M with laser irradiation, leading to a higher cytotoxic effect than either treatment alone or the combination of ZIF-8@Ver and laser (Figure 3A). Comparable outcomes were observed when CAL-27 cells were exposed to both ZIF-8@Ver and ZIF-8@Ver-M1M, as evidenced by the Live/Dead kit staining assay. This assay employs Calcein as a green fluorescent indicator for live cells and propidium iodide (PI) as a red fluorescent indicator for dead cells. In the groups treated with Verteporfin (Ver) and ZIF-8@Ver in conjunction with laser, distinct staining patterns were detected. The Live/Dead staining exhibited a reduction in the count of viable cells, indicated by reduced green fluorescence, compared to other groups without laser. Furthermore, in the ZIF-8@Ver-M1M-treated group, the Live/Dead staining showed predominantly red fluorescence, indicating the presence of a large number of dead cells. This suggests that ZIF-8@Ver-M1M treatment led to a notable reduction in cell viability, causing cell death (Figure 3B). The generation of reactive oxygen species (ROS) was measured to assess the therapeutic effect of PDT. ZIF-8@Ver-M1M-treated cells with laser exhibited a significant increase in intracellular ROS levels compared to other groups without laser (Figure 3C). ROS levels were further enhanced upon laser irradiation, indicating the synergistic effect of PDT and laser therapy.

These in vitro experiments provide strong evidence supporting the antitumor potential of ZIF-8@Ver-M1M, especially in combination with laser irradiation. The findings suggest that ZIF-8@Ver-M1M can promote ROS generation, inhibit cancer cell growth, and induce cell death, making it a promising candidate for photodynamic therapy in the treatment of cancer.

In vivo Tracking of Nano-Photosensitizer

The therapeutic effects of ZIF-8@Ver-M1M were assessed in nude mice with CAL-27 cell-bearing tumors. Tumors were established by injecting CAL-27 cells into the right shoulder of the mice. Upon reaching a tumor volume of 150 mm^3, the mice received treatment. The biodistribution investigation revealed that the fluorescence signal predominantly localized to the tumor region, signifying the accumulation of the nano-photosensitizer at the tumor sites. Moreover, ZIF-8@Ver-M1M nanoparticles exhibited preferential accumulation in the tumor tissues compared to Ver or ZIF-8@Ver (Figure 4A). The accumulation can be attributed to the specificity of M1 macrophage membranes, which allows the nano-photosensitizer binding to the cancer cells. In addition to the tumor, low levels of fluorescence were observed in other organs such as the livers, spleens, and kidneys (Figure 4B and C). There are ignorable fluorescence signals in the major organs, such as heart, liver, lung, spleen, or kidney, implying that the in situ injection of the nano-photosensitizer will be safe for the oral cancer therapy.

The cumulative release of ZIF-8@Ver-M1M nanoparticles was evaluated in both neutral (pH 7.4) and acidic (pH 5.4) environments to assess their drug release behavior under different conditions. In the neutral pH 7.4 environment, a sustained release pattern was observed, with a gradual increase in the cumulative release of Verteporfin over time. In contrast, in the acidic pH 5.4 environment, an accelerated release of Verteporfin was observed (Figure 4D). The acidic environment simulated the tumor microenvironment, which is known to be more acidic compared to normal tissues. This accelerated release can be attributed to the pH-responsive characteristics of ZIF-8-based nanoparticles, where the acidic conditions trigger the degradation or dissolution of the nanoparticles, leading to faster drug release.

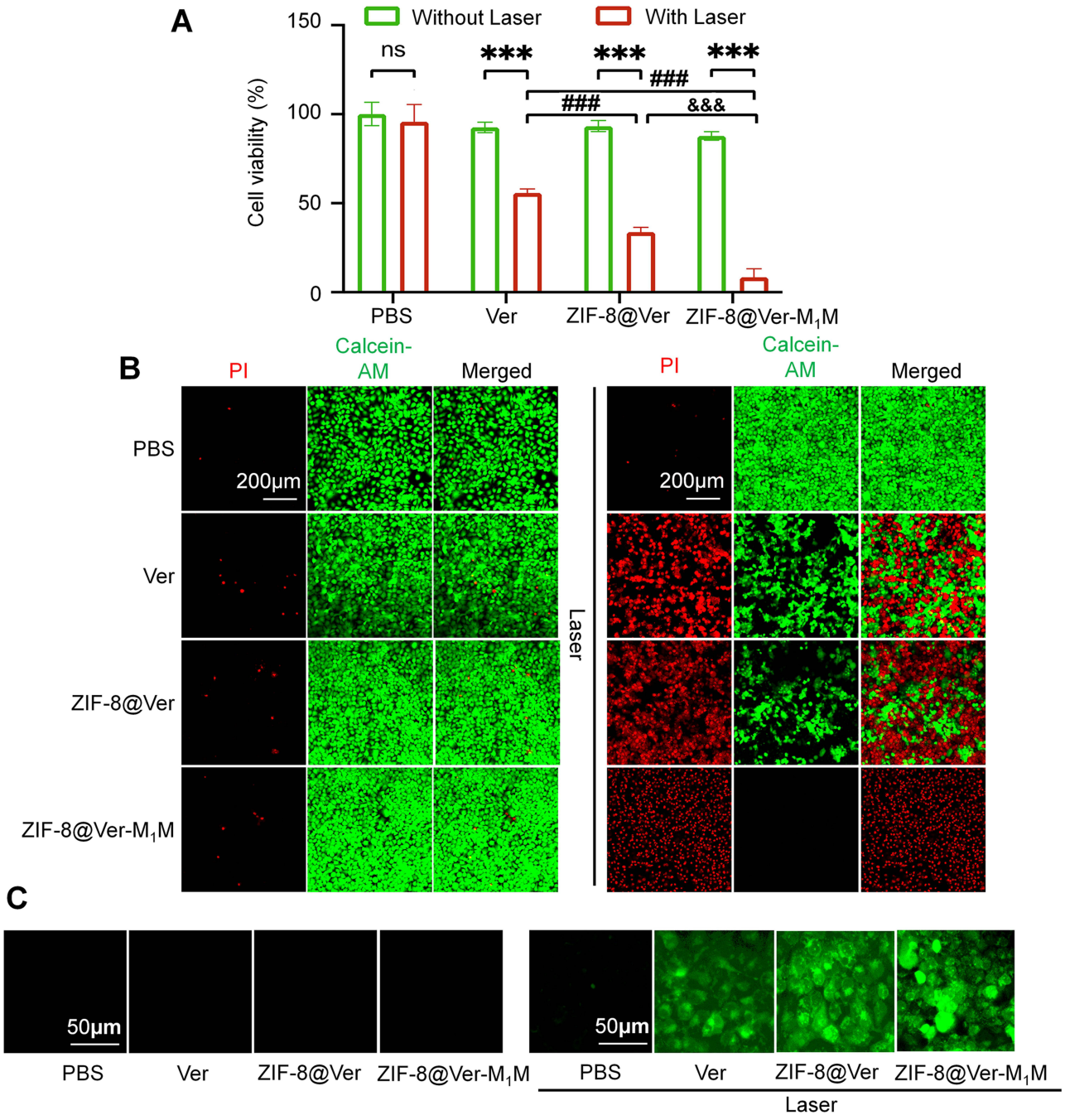

Figure 3 In vitro cytotoxicity study, calcein AM/PI staining analysis and ROS levels. CAL-27 cells were treated with PBS, Ver, ZIF-8@Ver, and ZIF-8@Ver-M1M for 4 h, with or without irradiation by 660 nm laser, respectively. (**A**) Cell viability of CAL-27 cells by CCK8 assay. (**B**) Fluorescence images of Calcein AM/PI-stained CAL-27 cells. (**C**) Determination of cellular ROS by DCFDA assay. ***$P < 0.001$ vs without laser group; $^{###}P < 0.001$ vs Ver+laser group; $^{&&&}P < 0.001$ vs ZIF-8@Ver-M1M+laser group.

In vivo Antitumor Effects

The therapeutic effects of ZIF-8@Ver-M1M were assessed in nude mice with CAL-27 cell-bearing tumors. The mice were treated with PBS, Ver, ZIF-8@Ver, ZIF-8@Ver-M1M, ZIF-8@Ver + laser, and ZIF-8@Ver-M1M + laser every two days for a duration of 20 days (Figure 5A), respectively. The tumor volumes were regularly monitored throughout the treatment period. Additionally, Ver, ZIF-8@Ver, or ZIF-8@Ver-M1M without laser demonstrated no significant inhibitory effects on tumor growth, as observed from the size and weight of extracted tumors and the monitored tumor volume (Figure 5B-D). The antitumor effect of ZIF-8@Ver and ZIF-8@Ver-M1M upon laser irradiation was superior to that in

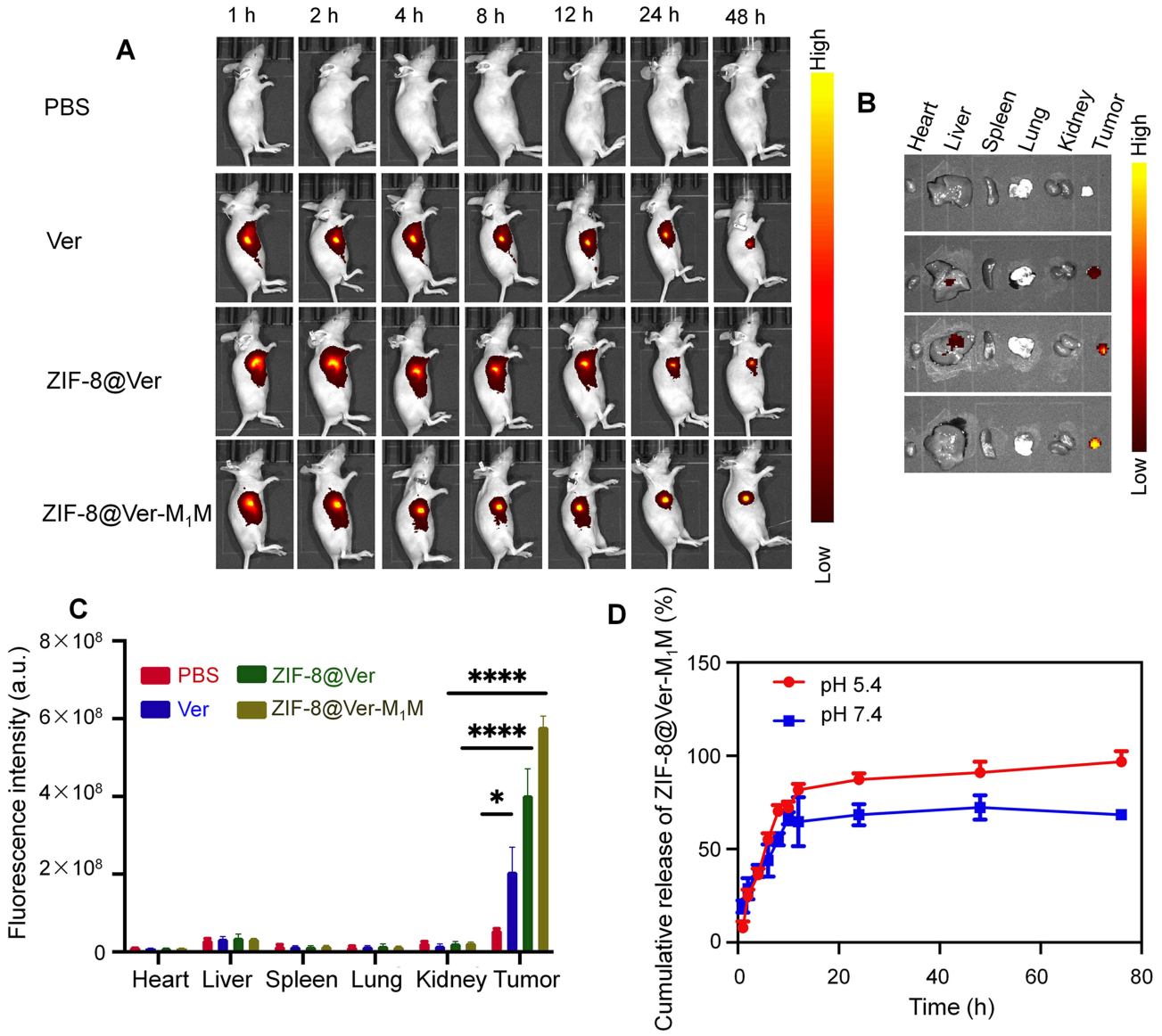

Figure 4 In vivo evaluation of biodistribution and the homotypic targeting. (**A**) In vivo biodistribution of fluorescent nanoparticles. (**B** and **C**) Ex-vivo imaging of major organs and quantitative assessment. The BALB/c mice were administrated with Ver, ZIF-8@Ver or ZIF-8@Ver-M1M, respectively (n = 3). (**D**) The cumulative release of ZIF-8@Ver-M1M in a neutral and acidic environment. *$P < 0.05$; ****$P < 0.0001$.

any other group. Notably, ZIF-8@Ver-M1M exhibited even greater suppression of tumor growth compared to uncoated ZIF-8@Ver. The administration of MOF-based nanoparticles did not result in significant changes in body weight (Figure 5E). As anticipated, noticeable necrotic areas were evident in tumor tissues following laser irradiation in the ZIF-8@Ver and ZIF-8@Ver-M1M treatment groups, whereas the control groups displayed minimal necrosis (Figure 5F). Immunohistochemical staining of tumor tissues unveiled a decline in Ki-67 expression, signifying decreased tumor cell proliferation in the ZIF-8@Ver-M1M and laser-treated group in comparison to the other groups without laser treatment (Figure 5F). The results from the TUNEL assay consistently demonstrated that ZIF-8@Ver and ZIF-8@Ver-M1M upon laser irradiation led to higher percentages of apoptotic cells compared to the unirradiated group (Figure 5F). Furthermore, no significant histological changes in major organs were observed following all treatments. (Figure S1), indicating minimal systemic toxicity. The in vivo assessment of tumor inhibition revealed that M1-membrane camouflaged nanoparticles enhanced the therapeutic efficacy of Verteporfin. These results point towards an encouraging and innovative approach in the field of cancer treatment.

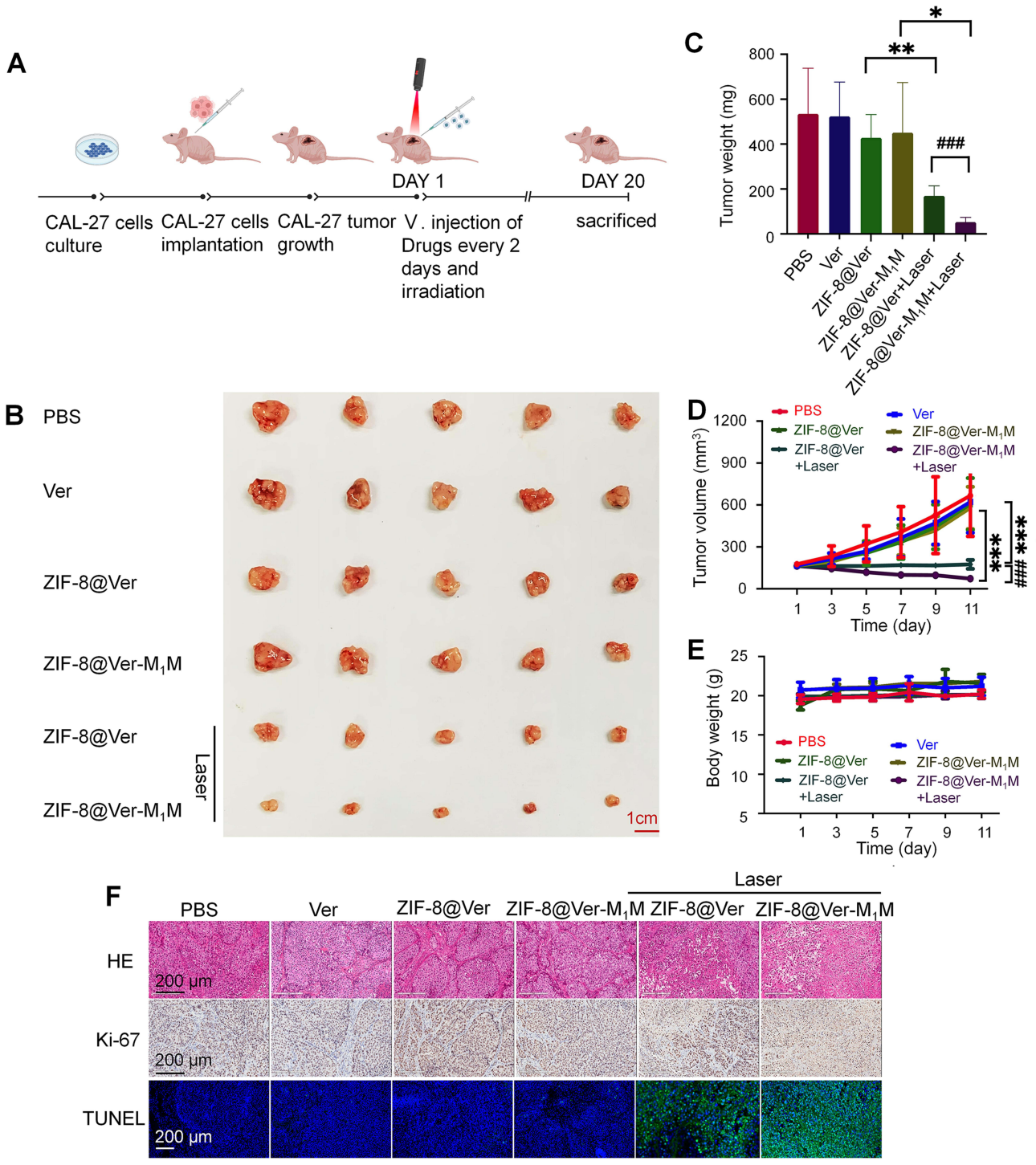

Figure 5 In vivo antitumor effects in nude mice bearing CAL-27 tumors following subcutaneous injection of PBS, Ver, ZIF-8@Ver, ZIF-8@Ver-M1M, ZIF-8@Ver + laser, and ZIF-8@Ver-M1M + laser (n=5). The mice were administered at an equivalent dose of Ver (20 mg/kg). (**A**) Illustration of photothermal therapy in nude mice; (**B**) The extracted tumors after different treatments; (**C**) The changes of tumor volume; (**D**) Tumor weights at the end of therapy on day 20; (**E**) The changes of body weight; (**F**) Representative histological images of tumor tissues stained with H&E, Ki-67, and TUNEL, respectively. **P* < 0.05; ***P* < 0.01; ****P* < 0.001; ###*P* < 0.001.

Discussion

Photodynamic therapy has emerged as a promising approach for cancer treatment.[26,27] In this study, we investigated the potential of using Verteporfin, a photosensitizer, for PDT of oral cancer. To improve the tumor targeting and enhance its

therapeutic efficacy, we developed a bioinspired nano-photosensitizer by using ZIF-8 as a carrier to load Verteporfin, which was camouflaged with M1 macrophage-derived cell membranes.

The use of macrophage membranes for nanoparticle coating provides several advantages supported by robust evidence. Macrophages possess effective tumor-targeting capabilities through the interaction between integrins α4β1 on M1 macrophage membranes and vascular cell-adhesion molecule 1 (VCAM-1) on tumor cell membranes.[28] Our results demonstrate that incorporating macrophage membranes onto nanoparticles exploits this tumor-targeting property, significantly enhancing nanoparticle accumulation in tumor tissues. This strategy elevates the local concentration of verteporfin, resulting in markedly improved photodynamic therapy (PDT) effects.

Furthermore, macrophage membrane coating acts as camouflage, enabling nanoparticles to evade immune recognition and clearance.[29,30] Our results substantiate that disguising nanoparticle with macrophage membranes prolongs circulation time and enhances their tumor accumulation. This is crucial for overcoming immune clearance, which often limits the efficacy of nanoparticle-based therapies.

The selection of ZIF-8 as the nanoparticle framework was based on its favorable drug delivery properties. Our study demonstrated that ZIF-8's porous structure provides a high surface area and loading capacity for verteporfin, ensuring efficient loading and controlled release of the drug in the tumor microenvironment. Additionally, ZIF-8 exhibits good stability and biocompatibility, ensuring the safety of the nanoparticles in vivo.[31–33]

Importantly, our experimental outcomes confirm that macrophage-membrane-coated ZIF-8 nanoparticles effectively delivered verteporfin to the tumor site. PDT treatment with these nanoparticles exhibited superior therapeutic effects compared to free verteporfin or uncoated nanoparticles, showcasing the synergistic effects of PDT. This enhanced efficacy resulted in significant inhibition of oral cancer. Notably, our findings highlight minimal systemic toxicity of macrophage-membrane-coated ZIF-8 nanoparticles, emphasizing their biocompatibility and safety. Biodistribution analysis indicated predominant accumulation in tumors with negligible histological changes in major organs, supporting the potential clinical translation of these nanoparticles.

Conclusion

In conclusion, our study developed a bioinspired nano-photosensitizer, which was constructed using ZIF-8 to load the clinically used Verteporfin, and further camouflaged with M1 macrophages-derived cell membranes. This type of nano-photosensitizer showed enhanced specificity and induced efficient PDT both in vitro and in vivo. The bioinspired nano-photosensitizer also showed effective inhibition of oral cancer by the effective PDT effect induced by Verteporfin. Further investigations are warranted to optimize the nanoparticle design, evaluate their efficacy in various cancer models, and explore their potential in clinical settings.

Abbreviations

PDT, Photodynamic therapy; MOFs, Metal-organic frameworks; ZIF-8, Zeolitic imidazolate framework 8; TEM, Transmission electron microscopy; CLSM, Confocal laser scanning microscopy; FBS, Fetal bovine serum; ROS, Reactive oxygen species; DCFH-DA, 2',7'-Dichlorodihydrofluorescein diacetate; PBS, Phosphate buffer saline; TSCC, Tongue squamous cell carcinoma; AMD, Age-related macular degeneration; PDI, Polydispersity index; UV-Vis, Ultraviolet-visible; ZIF-8@Ver, ZIF-8-loaded Verteporfin; BCA, Bicinchoninic acid; ZIF-8@Ver-M1M, M1 macrophages membranes coated ZIF-8@Ver; SDS-PAGE, Sodium dodecyl sulfate-polyacrylamide gel electrophoresis; LC, Loading content; FACS, Flow cytometry; HE, Hematoxylin-eosin; TUNEL, TdT-mediated dUTP nick-end labeling; CCK-8, Cell counting kit-8; PI, Propidium iodide; VCAM-1, Vascular cell-adhesion molecule 1.

Acknowledgments

This study was supported by the National Natural Science Foundation of China (No. 82000080), Guangzhou Health Science and Technology Project (20221A011102), Guangzhou Higher Education Teaching Quality and Teaching Reform Project-Excellent Talent Training Program (2022ZXRCPR008), and Guangdong Medical Research Foundation (A2023261). This work was also supported by the Plan on enhancing scientific research in Guangzhou Medical University (02-410-2302377XM). In addition, this study was supported by the Peak Discipline construction project of

Guangzhou Medical University-Epigenetic Drug Development Project (02-445-2301220XM, 02-445-2301164XM), and First-class professional construction project of Guangzhou Medical University (02-408-2304-13029XM).

Disclosure

The authors report no conflicts of interest in this work.

References

1. Mannelli G, Arcuri F, Agostini T, et al. Classification of tongue cancer resection and treatment algorithm. *J Surg Oncol*. 2018;117(5):1092–1099. doi:10.1002/jso.24991
2. Sagheb K, Kumar V, Rahimi-Nedjat R, et al. Cervical Metastases Behavior of T1-2 Squamous Cell Carcinoma of the Tongue. *J Maxillofac Oral Surg*. 2017;16(3):300–305. doi:10.1007/s12663-016-0936-0
3. Martin D, Degese MS, Vitale-Cross L, et al. Assembly and activation of the Hippo signalome by FAT1 tumor suppressor. *Nat Commun*. 2018;9(1):2372. doi:10.1038/s41467-018-04590-1
4. Giraud J, Molina-Castro S, Seeneevassen L, et al. Verteporfin targeting YAP1/TAZ-TEAD transcriptional activity inhibits the tumorigenic properties of gastric cancer stem cells. *Int J Cancer*. 2020;146(8):2255–2267. doi:10.1002/ijc.32667
5. Liu K, Du S, Gao P, et al. Verteporfin suppresses the proliferation, epithelial-mesenchymal transition and stemness of head and neck squamous carcinoma cells via inhibiting YAP1. *J Cancer*. 2019;10(18):4196–4207. doi:10.7150/jca.34145
6. Huggett MT, Jermyn M, Gillams A, et al. Phase I/II study of verteporfin photodynamic therapy in locally advanced pancreatic cancer. *Br J Cancer*. 2014;110(7):1698–1704. doi:10.1038/bjc.2014.95
7. Perra A, Kowalik MA, Ghiso E, et al. YAP activation is an early event and a potential therapeutic target in liver cancer development. *J Hepatol*. 2014;61(5):1088–1096. doi:10.1016/j.jhep.2014.06.033
8. Chen H-Y, Deng J, Wang Y, et al. Hybrid cell membrane-coated nanoparticles: a multifunctional biomimetic platform for cancer diagnosis and therapy. *Acta Biomater*. 2020;112:1–13. doi:10.1016/j.actbio.2020.05.028
9. Fang RH, Gao W, Zhang L. Targeting drugs to tumours using cell membrane-coated nanoparticles. *Nat Rev Clin Oncol*. 2023;20(1):33–48. doi:10.1038/s41571-022-00699-x
10. Zhou J, Tang Z, Gao S, et al. Tumor-Associated Macrophages: recent Insights and Therapies. *Front Oncol*. 2020;10:188. doi:10.3389/fonc.2020.00188
11. Zhang Y, Cai K, Li C, et al. Macrophage-Membrane-Coated Nanoparticles for Tumor-Targeted Chemotherapy. *Nano Lett*. 2018;18(3):1908–1915. doi:10.1021/acs.nanolett.7b05263
12. Yu Y, Song M, Chen C, et al. Bortezomib-Encapsulated CuS/Carbon Dot Nanocomposites for Enhanced Photothermal Therapy via Stabilization of Polyubiquitinated Substrates in the Proteasomal Degradation Pathway. *ACS Nano*. 2020;14(8):10688–10703. doi:10.1021/acsnano.0c05332
13. Liu C, Zhang W, Li Y, et al. Microfluidic Sonication To Assemble Exosome Membrane-Coated Nanoparticles for Immune Evasion-Mediated Targeting. *Nano Lett*. 2019;19(11):7836–7844. doi:10.1021/acs.nanolett.9b02841
14. Yang B, Ding L, Yao H, et al. A Metal-Organic Framework (MOF) Fenton Nanoagent-Enabled Nanocatalytic Cancer Therapy in Synergy with Autophagy Inhibition. *Adv Mater*. 2020;32(12):e1907152. doi:10.1002/adma.201907152
15. Liang S, Xiao X, Bai L, et al. Conferring Ti-Based MOFs with Defects for Enhanced Sonodynamic Cancer Therapy. *Adv Mater*. 2021;33(18):e2100333. doi:10.1002/adma.202100333
16. Kalaj M, Bentz KC, Ayala S, et al. MOF-Polymer Hybrid Materials: from Simple Composites to Tailored Architectures. *Chem Rev*. 2020;120(16):8267–8302. doi:10.1021/acs.chemrev.9b00575
17. Sun X, He G, Xiong C, et al. One-Pot Fabrication of Hollow Porphyrinic MOF Nanoparticles with Ultrahigh Drug Loading toward Controlled Delivery and Synergistic Cancer Therapy. *ACS Appl Mater Interfaces*. 2021;13(3):3679–3693. doi:10.1021/acsami.0c20617
18. Gao C, Huang Q, Liu C, et al. Treatment of atherosclerosis by macrophage-biomimetic nanoparticles via targeted pharmacotherapy and sequestration of proinflammatory cytokines. *Nat Commun*. 2020;11(1):2622. doi:10.1038/s41467-020-16439-7
19. Pan X, Wang W, Huang Z, et al. MOF-Derived Double-Layer Hollow Nanoparticles with Oxygen Generation Ability for Multimodal Imaging-Guided Sonodynamic Therapy. *Angew Chem Int Ed Engl*. 2020;59(32):13557–13561. doi:10.1002/anie.202004894
20. Chen Y, Li P, Modica JA, et al. Acid-Resistant Mesoporous Metal-Organic Framework toward Oral Insulin Delivery: protein Encapsulation, Protection, and Release. *J Am Chem Soc*. 2018;140(17):5678–5681. doi:10.1021/jacs.8b02089
21. Terzopoulou A, Wang X, Chen X-Z, et al. Biodegradable Metal-Organic Framework-Based Microrobots (MOFBOTs). *Adv Health Mater*. 2020;9(20):e2001031. doi:10.1002/adhm.202001031
22. Carrillo-Carrión C, Martínez R, Navarro Poupard MF, et al. Aqueous Stable Gold Nanostar/ZIF-8 Nanocomposites for Light-Triggered Release of Active Cargo Inside Living Cells. *Angew Chem Int Ed Engl*. 2019;58(21):7078–7082. doi:10.1002/anie.201902817
23. Li H, Peng Q, Yang L, et al. High-Performance Dual Combination Therapy for Cancer Treatment with Hybrid Membrane-Camouflaged Mesoporous Silica Gold Nanorods. *ACS Appl Mater Interfaces*. 2020;12(52):57732–57745. doi:10.1021/acsami.0c18287
24. Wang S, Li F, Qiao R, et al. Arginine-Rich Manganese Silicate Nanobubbles as a Ferroptosis-Inducing Agent for Tumor-Targeted Theranostics. *ACS Nano*. 2018;12(12):12380–12392. doi:10.1021/acsnano.8b06399
25. Zhang Y, Yang L, Wang H, et al. Bioinspired metal–organic frameworks mediated efficient delivery of siRNA for cancer therapy. *Chem Eng J*. 2021;426:131926. doi:10.1016/j.cej.2021.131926
26. Pham TC, Nguyen V-N, Choi Y, et al. Recent Strategies to Develop Innovative Photosensitizers for Enhanced Photodynamic Therapy. *Chem Rev*. 2021;121(21):13454–13619. doi:10.1021/acs.chemrev.1c00381
27. Agostinis P, Berg K, Cengel KA, et al. Photodynamic therapy of cancer: an update. *CA Cancer J Clin*. 2011;61(4):250–281. doi:10.3322/caac.20114
28. Li H, Li S, Lin Y, et al. Artificial exosomes mediated spatiotemporal-resolved and targeted delivery of epigenetic inhibitors. *J Nanobiotechnology*. 2021;19(1):364. doi:10.1186/s12951-021-01107-9

29. Oroojalian F, Beygi M, Baradaran B, et al. Immune Cell Membrane-Coated Biomimetic Nanoparticles for Targeted Cancer Therapy. *Small*. 2021;17 (12). doi:10.1002/smll.202006484
30. Lopes J, Lopes D, Pereira-Silva M, et al. Macrophage Cell Membrane-Cloaked Nanoplatforms for Biomedical Applications. *Small Methods*. 2022;6 (8):e2200289. doi:10.1002/smtd.202200289
31. Troyano J, Carné-Sánchez A, Avci C, et al. Colloidal metal-organic framework particles: the pioneering case of ZIF-8. *Chem Soc Rev*. 2019;48 (23):5534–5546. doi:10.1039/C9CS00472F
32. Qiu J, Tomeh MA, Jin Y, et al. Microfluidic formulation of anticancer peptide loaded ZIF-8 nanoparticles for the treatment of breast cancer. *J Colloid Interface Sci*. 2023;642:810–819. doi:10.1016/j.jcis.2023.03.172
33. Yang L, Lin Y, Zhang J, et al. Biomimetic metal-organic frameworks navigated biological bombs for efficient lung cancer therapy. *J Colloid Interface Sci*. 2022;625:532–543. doi:10.1016/j.jcis.2022.06.008